SUPPLEMENTAL FIGURES

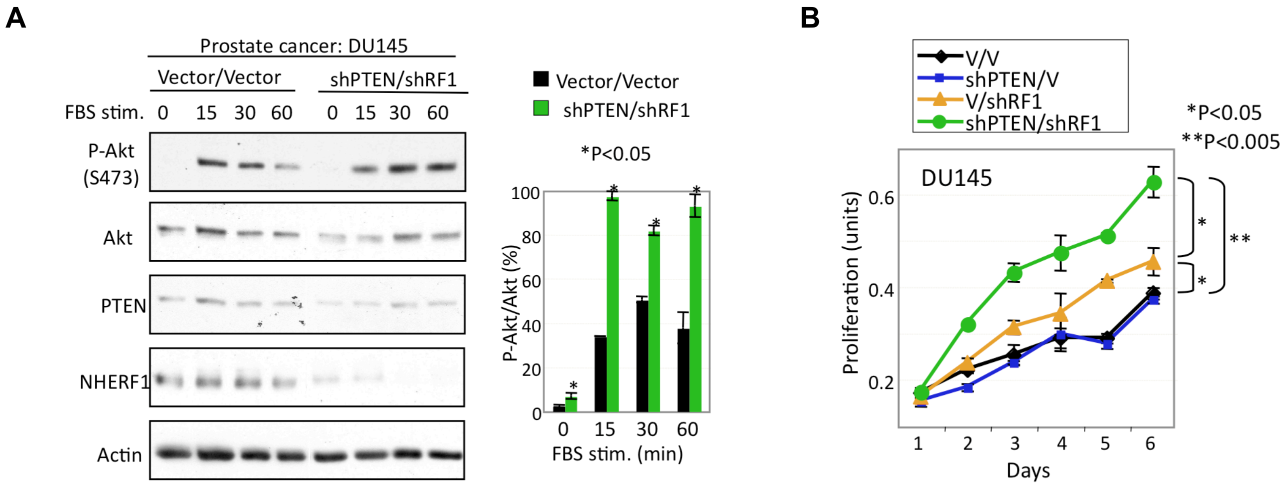

Fig. S1. Combined PTEN and NHERF1 loss synergistically activates Akt and increases proliferation in DU-145 prostate cancer cells. **A.** Time-course stimulation with 10% FBS of control and double silenced cells with shRNA for PTEN and NHERF1 (shRF1). **B.** MTT proliferation assay of control, single and double-depleted PTEN and NHERF1 cells.

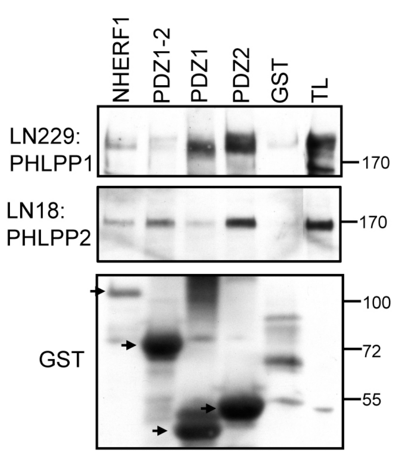

Fig. S2. Endogenous PHLPP1 interacts with both NHERF1 PDZ domains whereas endogenous PHLPP2 mainly interacts with NHERF1 PDZ2 domain. GST pull-down with the GST-NHERF1 protein battery from Fig. 1B of proteins from total lysates (TL) obtained from LN229 and LN18 glioblastoma cell lines, as indicated. The filters were re-probed with GST antibody to show similar amounts of GST-fusion proteins (arrows), including GST (not shown). GST-NHERF1 full length was used in significantly lower amount.

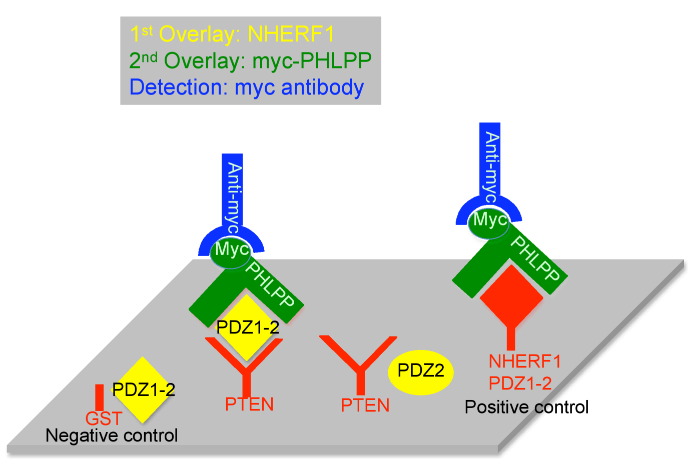

Fig. S3. Cartoon of the bridging overlay assay. Filter-immobilized proteins (red) are overlaid in a first step with various bridging NHERF1 PDZ domains (yellow), in a second step, with Myc-tagged PHLPP proteins (green), and in a third step, with Myc antibody (blue). Immobilized GST (negative control) cannot bind any of the overlaid proteins. NHERF1 PDZ1-2 (positive control) binds directly to the PHLPP proteins. PTEN can bind NHERF1 PDZ1-2 or PDZ1 but not PDZ2.

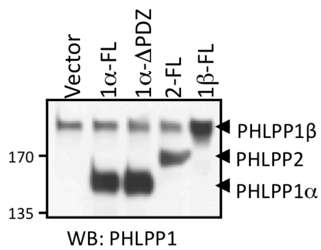

Fig. S4. Expression of the full length (FL) PHLPP isoforms in 293T cells (see scheme in Fig. 1C). The detection was carried out with anti-PHLPP1 antibody that recognizes also PHLPP2 with lower sensitivity than the anti-PHLPP2 specific antibody.

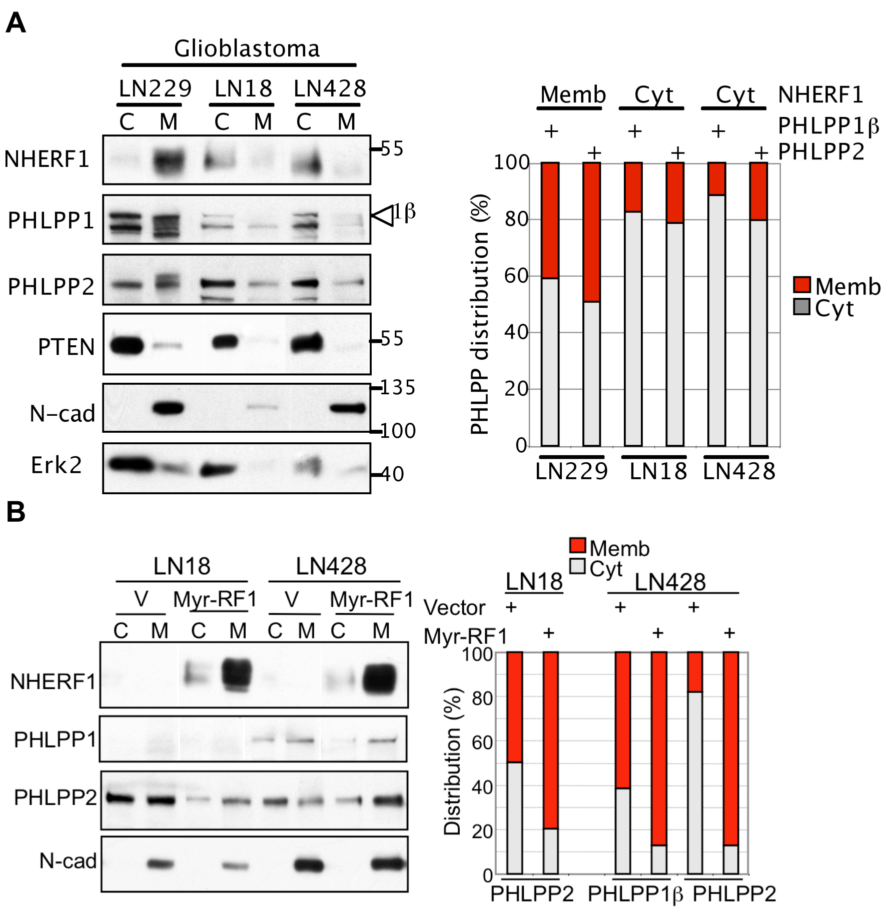

Fig. S5. NHERF1 recruits PHLPP1/2 to the membrane. **A.** Correlation between NHERF1, PHLPP and PTEN membrane distributions in glioblastoma cells. Fractionation in cytosolic (C) and membrane (M) fractions shows co-fractionation of NHERF1 with PHLPP1, PHLPP2 and PTEN. Erk2 and N-cadherin were used as cytosolic and membrane fractionation markers, respectively. The densitometric intensities of the cytoplasmic and membrane bands for PHLPP1β and PHLPP2 were represented graphically as % from the summed membrane and cytosolic distributions. **B.** Redistribution of endogenous PHLPP1β and PHLPP2 to the membrane by Myr-NHERF1 (Myr-RF1) as compared to vector (V) control cells.

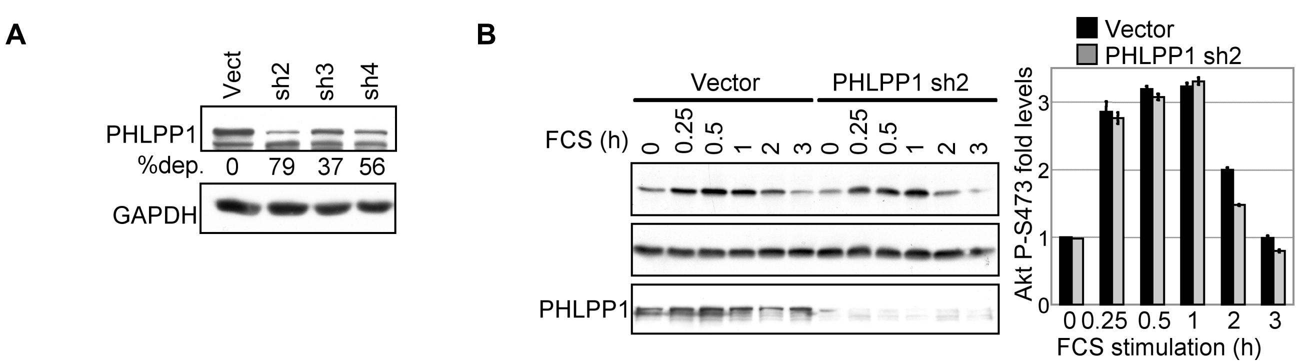

Fig. S6. PHLPP1 depletion does not lead to Akt activation in LN229 cells. **A.** PHLPP1β silencing by 3 shRNAs in LN229 cells shows best % depletion (dep.) by sh#2, followed by sh#4. PHLPP1 levels were normalized to GAPDH levels. **B.** Time course of 10% FBS stimulation in LN229 cells depleted of PHLPP1 does not show significant Akt phosphorylation vs. vector-control cells (p>0.05). Values are means±SEM from two independent experiments.

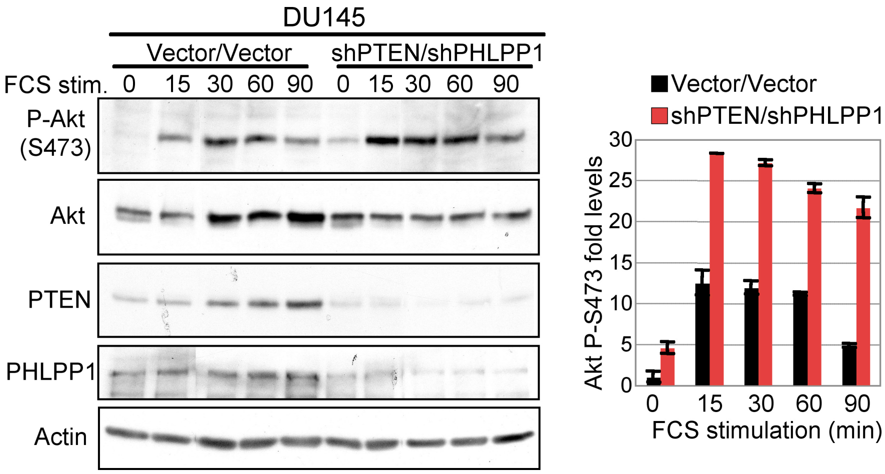

Fig. S7. Synergistic Akt activation by double PTEN and PHLPP1 silencing in DU-145 prostate cancer cells. Time-course stimulation with 10% FBS shows significantly increased Akt phosphorylation by double PTEN and PHLPP1 shRNA depletion. Values are means±SEM from two independent experiments. Statistical significant differences ($p<0.05$) were obtained for all time points between PTEN-PHLPP1-depleted vs. vector control cells.

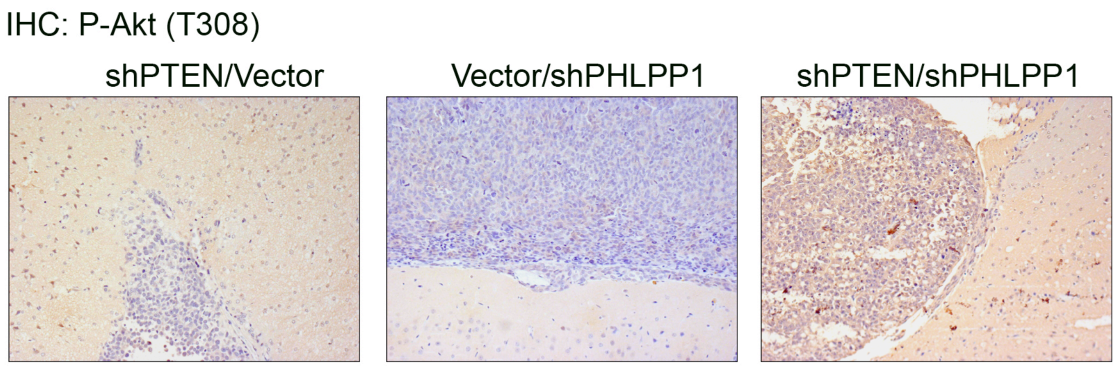

Fig. S8. Immunohistochemistry (IHC) staining (x200) of the tumors from Fig. 4D with phospho-Thr308 Akt antibody (Cell Signaling). Note pronounced P-Akt (T308) labeling of double shPTEN/shPHLPP1-depleted tumor cells in contrast with single shPTEN/Vector- or Vector/shPHLPP1-depleted cells. Note also infiltration of the brain parenchyma with shPTEN/Vector or shPTEN/shPHLPP1 tumor cells.

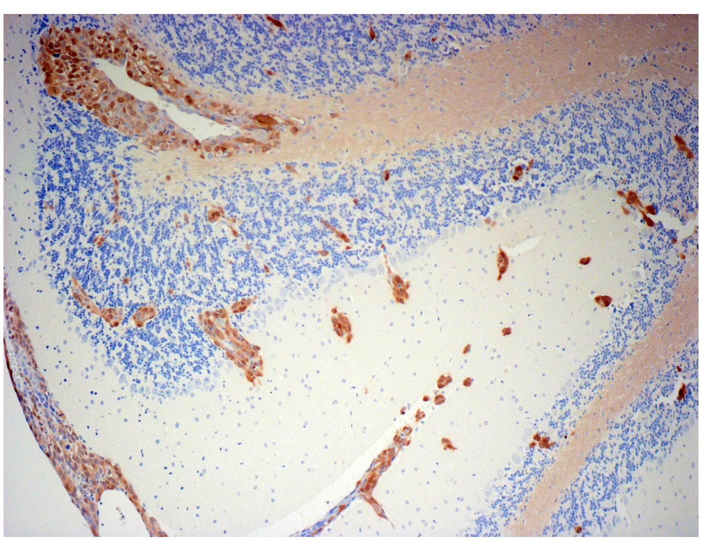

Fig. S9. PTEN depletion confers enhanced invasiveness to tumor cells. IHC staining with GFP antibody of brain sections from euthanized mice inoculated with shPTEN/Vector-depleted LN229 cells shows massive perivascular infiltration of large (upper left corner) and small blood vessels, infiltration of the meninges (lower left corner), and invasion of separate or clustered tumor cells into the white and gray matter.

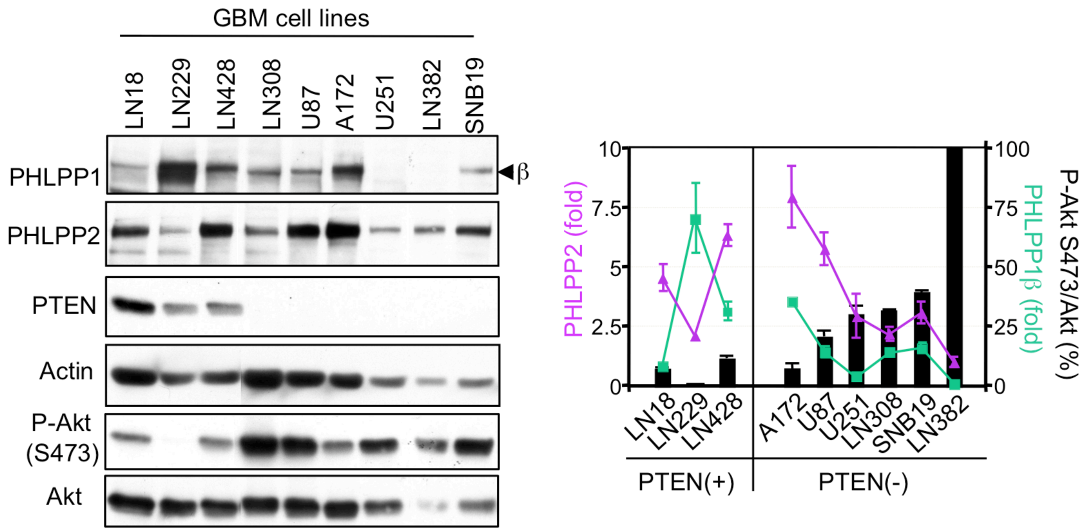

Fig. S10. PHLPP1 and PHLPP2 levels show inverse correlation with Akt activation in PTEN-negative glioblastoma (GBM) cell lines. Three PTEN-positive and six PTEN-negative glioblastoma cell lines were analyzed for PHLPP1 and PHLPP2 expression, and phosphorylated Akt (P-Akt) levels. The graph shows the levels of PHLPP1β, the major PHLPP1 isoform in cell lines, and PHLPP2, normalized to actin levels, superimposed on the corresponding P-Akt/Akt levels. Note significant inverse correlation between either PHLPP1β and P-Akt (r=-0.70) or PHLPP2 and P-Akt (r=-0.77) levels only in PTEN-negative cell lines.

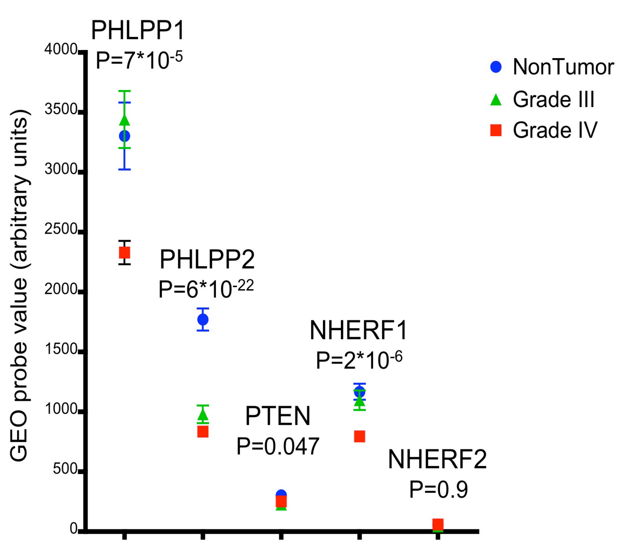

Fig. S11. Analysis of PHLPP1, PHLPP2, PTEN, NHERF1 and NHERF2 gene expression in the GSE4290 glioma datasets. The publically available GEO data (www.ncbi.nlm.nih.gov/projects/geo/) was mined. The GSE4290 dataset containing patient samples that include 23 brain samples from epilepsy patients used as non-tumor controls, 19 WHO grade III astrocytoma (low grade) and 81 WHO grade IV glioblastoma (high grade) was analyzed by using 5 probesets mapped to PHLPP1 (212719_at), PHLPP2 (213407_at), PTEN (233314_at), NHERF1 (201349_at) and NHERF2 (209830_s_at) (Affymetrix, Santa Clara, CA). A single glioblastoma sample, GSM97917 was identified as outlier and excluded from the analysis. Plots were generated using the arbitrary values provided for the probesets. The statistical analysis was performed as in Fig.5A and p-values are shown for glioblastoma vs. control. Note pronounced decrease of mRNA expression for PHLPP1, PHLPP2 and NHERF1 in glioblastoma compared to control samples, and no change for NHERF2, the homologue of NHERF1.